Optical characterization of spin-charge-orbital orders in $Pr(Sr_{1-y}Ca_y)_2Mn_2O_7$

I. Ishii
Department of Applied Physics, University of Tokyo, Tokyo 113-8656, Japan

Y. Tokunaga and J. Fujioka
Multiferroics Project, ERATO, Japan Science and Technology Agency (JST), Tokyo 113-8656, Japan

Y. Onose
Department of Applied Physics, University of Tokyo, Tokyo 113-8656, Japan
and Multiferroics Project, ERATO, Japan Science and Technology Agency (JST), Tokyo 113-8656, Japan

Y. Tokura
Department of Applied Physics, University of Tokyo, Tokyo 113-8656, Japan;
Multiferroics Project, ERATO, Japan Science and Technology Agency (JST), Tokyo 113-8656, Japan;
and Cross-Correlated Materials Research Group (CMRG) and Correlated Electron Research Group (CERG), Wako 351-0198, Japan
(Received 26 July 2010; revised manuscript received 12 October 2010; published 2 December 2010)

Bilayered-structure manganites $Pr(Sr_{1-y}Ca_y)_2Mn_2O_7$ show the competing spin-charge-orbital orders; the ground state is the spin CE-type charge-orbital ordered state for $y>0.4$ and the spin-A-type ferroic x^2-y^2 orbital ordered state for $y<0.4$. For the two representative crystals of $y=0.9$ and $y=0$, we have investigated the optical conductivity and Raman spectra to probe the charge, spin, and lattice dynamics of the respective phases. For $y=0.9$, the charge-orbital ordered states are characterized by strongly activated Raman phonon bands corresponding to the modulated breathing and Jahn-Teller lattice distortions, as observed commonly for other charge-orbital ordered manganites. As the unique features of this bilayered manganite, however, we found that the infrared-active phonon mode can also show up in the Raman spectra in the lower-temperature charge-orbital ordered state, confirming the breaking of centrosymmetry to produce the spontaneous electric polarization. The other feature to be noted is the appearance of the two-magnon excitation band of the CE-type spin order in the Raman spectra which estimates the energy scale of spin exchange energies. For $y=0$, on the other hand, we have observed a charge gap in the optical conductivity spectrum which becomes narrowed with the evolution of the A-type (in-plane ferromagnetic) spin order but remains finite (0.15 eV) at the ground state. The persistence of the charge gap is ascribed to the vertical charge ordering or charge-density wave (CDW) that was previously verified by diffuse x-ray scattering. Such charge-order or CDW formation also activates additional infrared phonon modes at 26 and 35 meV, whose spectral intensity appears to be enhanced by resonance with the underlying electronic continuum.

DOI: 10.1103/PhysRevB.82.245103 PACS number(s): 75.25.Dk, 78.30.−j

I. INTRODUCTION

The order-disorder phenomena of charge, orbital, and spin degrees of freedom are a central issue in physics of manganese oxides.[1] In a parent compound of perovskite manganite $LaMnO_3$, where all the Mn ions are trivalent, the electrons at the degenerate e_g orbital show the staggered $d_{3x^2-r^2}/d_{3y^2-r^2}$-type orbital ordering (OO) and A-type spin order (SO) (antiferromagnetically coupled ferromagnetic planes). By doping holes into $LaMnO_3$, the orbital quantum-disordered ferromagnetic metal is realized. In narrower band width systems (e.g., $Pr_{1-x}Ca_xMnO_3$), the charge-orbital ordered state with the CE-type spin order (CE-COO) (Refs. 2 and 3) emerges around a half doping level ($x\sim0.5$). In the ordered state, as shown in Figs. 1(d) and 1(e), the nominal Mn^{3+} and Mn^{4+} sites order alternatively like a checkerboard as the CO, $d_{3x^2-r^2}$ and $d_{3y^2-r^2}$ orbital stripes at Mn^{3+} sites are aligned along the diagonal direction, and the spins form ferromagnetic zigzag chain coupled antiferromagnetically with the neighboring chains, which is referred to as CE-type spin order. Colossal magnetoresistance[1] can be understood as induced by the competition between the charge-orbital ordered insulating state and the ferromagnetic metal state. In the high doping (x) range, the uniform $d_{x^2-y^2}$ OO with A-type spin ordered state, and the uniform $d_{3z^2-r^2}$ order with C-type (antiferromagnetically coupled ferromagnetic chain) SO successively show up as the two- and one-dimensional variants of the double-exchange ferromagnetism, respectively.[4,5]

The A-type antiferromagnetic state and the CE-COO are also realized in bilayered manganite compounds $R_{2-2x}A_{1+2x}Mn_2O_7$.[6–12] In addition, the two dimensionality of electronic and crystal structures endow the ordered states with unique natures. In Fig. 1(a), we show the electronic phase diagram of $Pr(Sr_{1-y}Ca_y)_2Mn_2O_7$.[13] The A-type AF and the CE-COO compete with each other in this system and are well separated from each other as a function of the Ca content (y). This is contrastive with the well-studied case of $La_{2-2x}Sr_{1+2x}Mn_2O_7$,[6,9,10] where the two phases coexist in the same doping region around $x=0.5$. In this context, the $Pr(Sr_{1-y}Ca_y)_2Mn_2O_7$ system is suited for the study of these charge-orbital-spin ordered states. While $PrSr_2Mn_2O_7$ has a tetragonal structure ($I4/mmm$, $a=b=3.8535$ Å and $c=19.928$ Å),[13] the Ca-doped ($y>0.4$) crystals have lower symmetry due to the tilting of MnO_6 octahedron around a

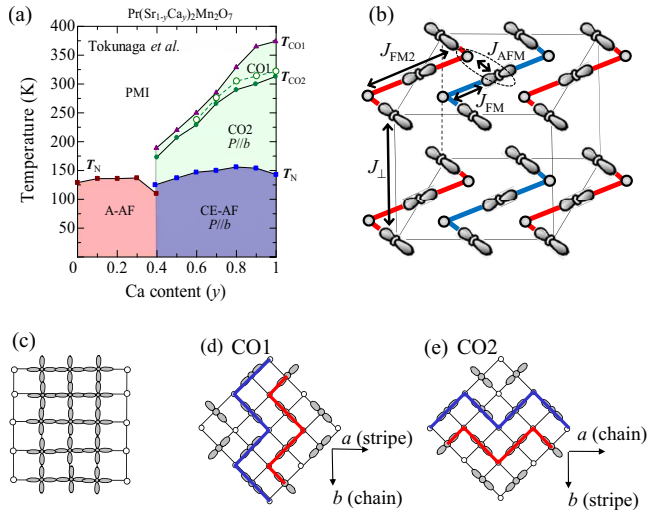

FIG. 1. (Color online) (a) Electronic phase diagram (Ref. 13) in $Pr(Sr_{1-y}Ca_y)_2Mn_2O_7$ as reproduced from Ref. 13. CO1 and CO2 are the two different charge-orbital ordered states as illustrated on (d) and (e), respectively. A-AF and CE-AF stand for A-type and CE-type antiferromagnetic states, respectively. The squares, triangles, and circles show transition temperatures determined from resistivity and magnetization measurements. The triangle indicates the transition temperature of CO1 state (T_{CO1}). The open and closed circles stand for the transition temperature T_{CO2} of CO2 state with thermal hysteresis. The squares show the Néel temperature T_N. (b) Schematic illustration of the spin-CE-type charge-orbital ordered pattern. J_{FM} and J_{AFM} stand for the ferromagnetic and antiferromagnetic interactions between the neighboring cites. $J_\perp$ is the interplane exchange interaction. (c) Schematic of charge-orbital ordered state with uniform x^2-y^2 orbital and vertical charge stripe-ordered state and schematics of the spin CE-type charge-orbital ordered states (d) With the orbital stripe along a axis and (e) with the orbital stripe along b axis. Thick lines in (d) and (e) stand for the ferromagnetic zigzag chains coupled antiferromagnetically.

axis (*Amam*, $a=5.4060$ Å, $b=5.4671$ Å, and $c=19.221$ Å for $PrCa_2Mn_2O_7$).[13] In this case, there are two possible arrangements of the CO-OO with respect to the orthorhombic crystal axis. Namely, the zigzag chain is parallel to the b axis [CO1, Fig. 1(d)] or the a axis [CO2, Fig. 1(e)]. These two types of orders are both observed in $Pr(Sr_{1-y}Ca_y)_2Mn_2O_7$ ($y>0.4$).[13] The CO1 is observed in a limited temperature range between T_{CO1} and T_{CO2} and the CO2 in a lower temperature region below T_{CO2}. Tokunaga *et al.*[14] reported the spontaneous electric polarization below T_{CO2} as probed by the second-harmonic generation measurement. In the A-type AF for $y<0.4$, on the other hand, the x-ray scattering measurement has revealed the short-range correlation of vertical stripe-type charge ordering with the $\sim 4a_0$ period (a_0 being the tetragonal cell parameter),[13] as shown in Fig. 1(c). A similar charge stripe order was also reported for $La_{2-2x}Sr_{1+2x}Mn_2O_7$ (Refs. 15 and 16) and the angle-resolved photoemission measurement suggests that the origin can be ascribed to the nesting of Fermi surface.[17]

The purpose of this paper is to investigate the variation in optical responses of half-doped ($x=0.5$) bilayer manganites upon their respective charge-spin-orbital phase transitions. Among various experimental probes, the optical spectroscopy can provide important information not only about the ordering but also about the dynamics in the charge, orbital, and spin sectors. For example, it uncovers the optical gap formation induced by the charge-orbital ordering, the anisotropic charge dynamics in the orbital ordered state and the activation and/or splitting of the phonon modes reflecting the broken lattice symmetry in the optical conductivity and the Raman spectra.[18,19] In this paper, we have investigated the infrared and Raman spectra of the CE-type SO state in $Pr(Sr_{0.1}Ca_{0.9})_2Mn_2O_7$ ($y=0.9$), and the A-type AF with vertical stripe charge order in $PrSr_2Mn_2O_7$($y=0$). We have observed the activation of infrared optical-phonon mode in the Raman spectra below T_{CO2} as an indication of the broken space-inversion symmetry. A two-magnon band has also been discerned in the CE-type SO, which enables us to estimate the spin exchange energy in the CE-type spin ordered state. In $PrSr_2Mn_2O_7$, on the other hand, the clear decrease in the charge gap occurs with evolution of the A-type spin order, while the activated phonon modes are observed below T_N due to the vertical stripe charge order. The consequence of such a charge order in charge dynamics is argued in terms of the optical conductivity spectra.

II. EXPERIMENTAL

Samples used in this work were single crystals of $Pr(Sr_{1-y}Ca_y)_2Mn_2O_7$ with $y=0$ and $y=0.9$ grown by a floating-zone method. The detailed procedure of the crystal growth is described elsewhere.[13] The Raman spectra were measured using a temperature variable cryostat and a triple-grating spectrometer equipped with a liquid-nitrogen-cooled charge-coupled-device detector. The 2.410 eV (514.5 nm) line from an Ar-ion laser was utilized for the excitation. The spot size of the laser for the excitation was about 4 μm in diameter. We collected the scattered light in backscattering configuration in the two polarized configurations: $(x'x')=(x+yx+y)$ and $(x'y')=(x+yx-y)$, where x' and y' correspond to the polarization of incident and/or scattered light and x, y correspond to the Mn-O direction on the ab (xy) plane. All the spectra were calibrated by the instrumental sensitivity. The temperature dependence of the reflectivity spectra at nearly normal incidence was measured for the xy plane between room temperature and 10 K in the energy region of 0.01–5 eV. In the photon energy region of 0.01–0.7 eV and 0.5–5 eV, we used a Fourier-transform spectrometer and a grating-type monochromator, respectively. The reflectivity spectra above 5 eV (up to 40 eV) were measured at room temperature with use of synchrotron radiation at UV-SOR, Institute of Molecular Science, Okazaki, and used for the Kramers-Kronig analysis to deduce the optical conductivity spectra.

III. RESULTS AND DISCUSSION

A. Charge orbital order in $Pr(Sr_{0.1}Ca_{0.9})_2Mn_2O_7$ with the CE-type magnetic ordering

In this section, we discuss the Raman and optical conductivity spectra for $Pr(Sr_{0.1}Ca_{0.9})_2Mn_2O_7$ showing the CE-COO ground state. The CO-OO emerges at $T_{CO1}=370$ K, the or-

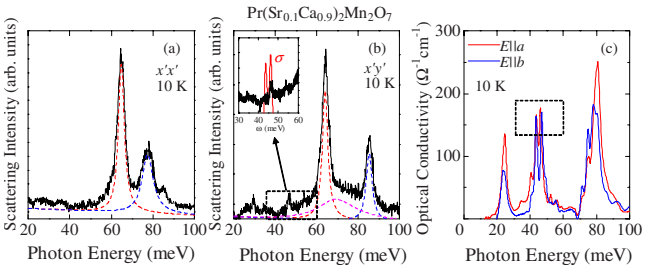

FIG. 2. (Color online) [(a) and (b)] Raman-scattering spectra in (a) $(x'x')$ and (b) $(x'y')$ configuration ($x'=a$, $y'=b$) at 10 K for $Pr(Sr_{0.1}Ca_{0.9})_2Mn_2O_7$ ($y=0.9$). (c) Optical conductivity spectra of phonon modes in $E\|a$ and $E\|b$ configurations at 10 K for the same crystal. Inset shows the comparison between the Raman spectrum and the optical conductivity spectrum at 10 K in the energy region represented by the dashed squares in (b) and (c).

bital stripe rotates by 90° at $T_{CO2}=300$ K, and then the antiferromagnetic order (CE-type) is realized at $T_N=150$ K. The CO-OO state below T_{CO2} is anticipated to have a finite spontaneous polarization.[14] Figure 2 shows the Raman spectra at 10 K in (a) $(x'x')$ configuration and (b) $(x'y')$ configuration for $Pr(Sr_{0.1}Ca_{0.9})_2Mn_2O_7$. Dashed lines represent the Lorentzian functions to fit the Raman peaks. Two phonon modes with large scattering intensity are observed at 64 and 77 meV in the $(x'x')$ Raman spectra, and at 64 and 85 meV in the $(x'y')$ Raman spectra. These four phonon modes were also observed in $La_{0.5}Sr_{1.5}MnO_4$ and $LaSr_2Mn_2O_7$ (Ref. 20) as well and activated by the lattice distortion accompanied by the CE-COO. The lower- and higher-lying peaks in both the $(x'x')$ and $(x'y')$ configurations can be ascribed to the Jahn-Teller and the breathing modes, respectively.[20] In Figs. 3(a) and 3(b), we show the temperature dependence of the Raman-scattering spectra with the $(x'x')$ and $(x'y')$ configurations for $Pr(Sr_{0.1}Ca_{0.9})_2Mn_2O_7$, Jahn-Teller and breathing phonon modes are activated below 350 K in each configura-

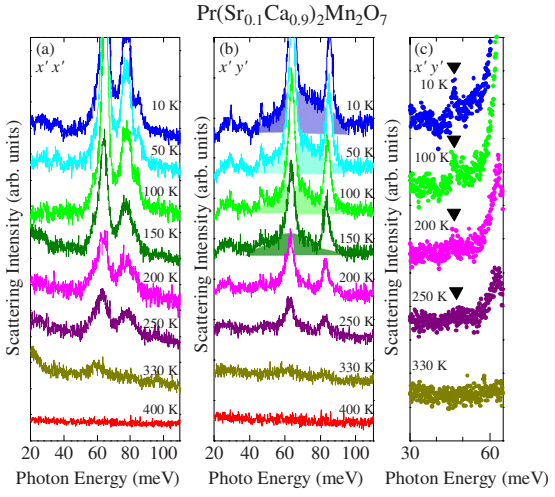

FIG. 3. (Color online) Temperature dependence of Raman-scattering spectra in (a) $(x'x')$ and (b) $(x'y')$ configurations for $Pr(Sr_{0.1}Ca_{0.9})_2Mn_2O_7$ ($y=0.9$). Shaded regions in (b) represent the broadbands caused by two-magnon excitation. (c) Magnified Raman spectra in $(x'y')$ configuration at various temperatures around the activated phonon mode at 46 meV.

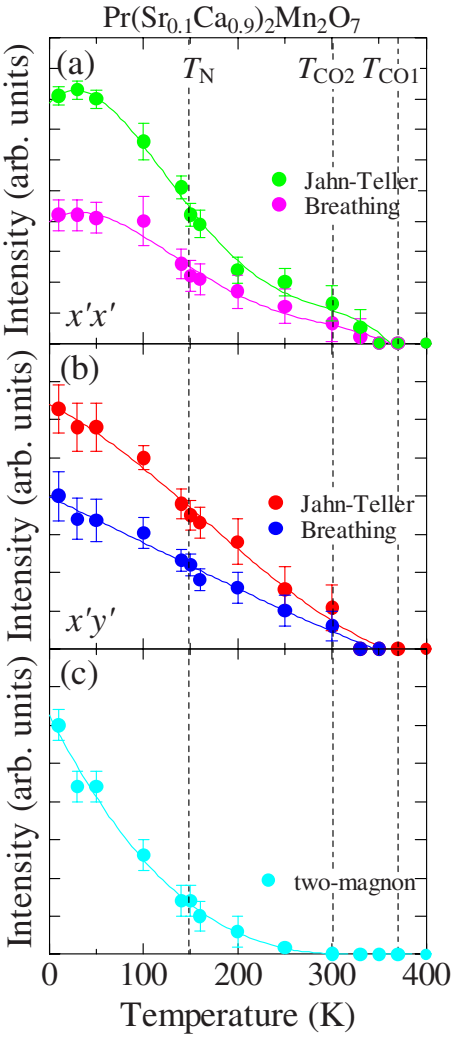

FIG. 4. (Color online) [(a) and (b)] Temperature dependence of intensity of Jahn-Teller and breathing modes in (a) $(x'x')$ and (b) $(x'y')$ Raman spectra, respectively, for $Pr(Sr_{0.1}Ca_{0.9})_2Mn_2O_7$ ($y=0.9$). (c) Temperature dependence of the intensity of the two-magnon excitation for the same crystal.

tion, and increase their intensities with decreasing temperature. Note that the gradual increase in background scattering intensity toward low frequency observed between 150 and 330 K in the $(x'x')$ configuration is due to the diffuse scattering caused by strong phase fluctuation in this system.[21,22] To discuss the quantitative aspect, we plot in Fig. 4 the temperature dependence of the scattering intensities of the Jahn-Teller and breathing modes as deduced from the fitting with Lorentzian function, as exemplified in Figs. 2(a) and 2(b) with dashed lines. In the $(x'y')$ configuration, the intensities of both the Jahn-Teller and breathing modes monotonically increase with decreasing temperature from T_{CO1}. On the other hand, the intensities in the $(x'x')$ configuration increase rapidly toward low temperature from T_N. Since the lattice parameter does not show any discernible anomaly around T_N,[23] the anomaly around T_N cannot be explained in terms of the change in the lattice sector alone. This might imply the hybridization of the phonon modes with orbital excitations that are governed by the magnetic order.[24]

In the $(x'y')$ configuration, we observed an additional broadband in the energy region of 50–90 meV as indicated by a dashed line centered at 70 meV in Fig. 2(b). As presented in Fig. 3(b), this broadband (shaded area) emerges below 150 K and grows as temperature is lowered. In Fig. 4(c), we show the temperature dependence of the scattering intensities of the broadband estimated by the integration of the shaded region, i.e., the integration of the scattering intensity between 35 and 100 meV after subtraction of phonon modes and constant background. Since the spectral intensity develops from T_N, this broadband is likely assigned to a two-magnon excitation which arises from the spin exchange process between the antiferromagnetically coupled nearest-neighboring spins. In the tetragonal lattice with D_{4h} symmetry, the two-magnon excitation would be of B_{1g} symmetry and active in the $(x'y')$ configuration.[25] While it is difficult to consider the full crystal symmetry of spin-CE-type charge-orbital order, the dominant component of the two-magnon excitation is expected in the $(x'y')$ configuration even in the present system with lower crystal symmetry. In fact, the two-magnon excitations have been reported in this polarization configuration in several charge- and/or orbital-ordered layered transition-metal oxides.[26–28] In general, the energy of two-magnon excitation is known to roughly coincide with the energy cost of the neighboring spin exchange process. In the present case, the energy cost of the spin exchange process between the antiferromagnetically coupled neighboring Mn^{3+} and Mn^{4+} cites in the spin-CE-type COO, as indicated by a dashed circle in Fig. 1(b), is

$$7J_{\mathrm{FM}} + \frac{7}{2}J_{\mathrm{AFM}} + \frac{3}{2}J_{FM2} + \frac{7}{2}J_{\perp}. \quad (1)$$

Here J_{FM}, J_{FM2}, J_{AFM}, and $J_{\perp}$ are the nearest-neighbor ferromagnetic exchange interaction, the second-nearest-neighbor ferromagnetic exchange interaction, the antiferromagnetic exchange interaction between the neighboring chain, and the interlayer antiferromagnetic exchange interaction, respectively, as indicated in Fig. 1(b). For a CE-type spin order in the single-layered manganese oxide $La_{0.5}Sr_{1.5}MnO_4$,[29] the magnitudes of the exchange interactions were estimated by the inelastic neutron measurement of the spin excitation as $J_{\mathrm{FM}}=9.98$ meV, $J_{\mathrm{FM2}}=3.69$ meV, and $J_{\mathrm{AFM}}=1.83$ meV. If we assume that these magnitudes are the same for bilayered manganites and $J_{\perp}=J_{\mathrm{AFM}}$, the energy cost of the spin exchange process is 88 meV. This is comparable with the observed two-magnon energy ($\simeq$70 meV), assuring the present interpretation of the two-magnon band.

Figure 2(c) shows the optical conductivity spectra at 10 K in the low-energy region ($<$100 meV) with $E\|a$ and $E\|b$ configurations. In the perovskite related structure,[30,31] the infrared phonon spectra is composed of stretching, bending, and external modes. The lowest energy mode around 25 meV can be ascribed to the external mode relevant to the vibration of rare-earth ions. The phonon modes around 45 meV and around 80 meV are bending and stretching mode, respectively, but split by the lowered lattice symmetry due to the COO.[13,14] Similar split and/or activated modes are observed for many CO transition systems in the perovskite structure,[31–33] including the CE-COO state of manganite.[34]

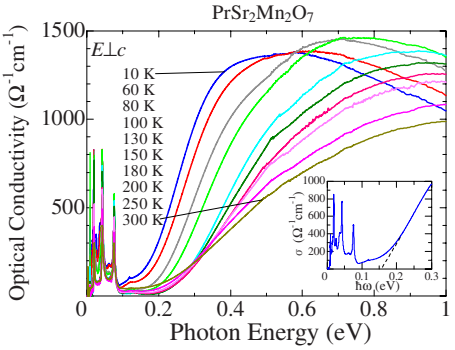

FIG. 5. (Color online) Optical conductivity spectra for $PrSr_2Mn_2O_7$ $(y=0)$ at various temperatures. The inset exemplifies the extrapolation procedure to estimate the charge gap magnitude.

Inset in Fig. 2(b) compares the optical conductivity spectrum with the Raman spectrum in the region indicated by dashed squares in Figs. 2(b) and 2(c). In the Raman spectrum, a weak but discernible phonon mode is observed at 46 meV, where the Mn-O bending mode is observed in the optical conductivity spectrum. The temperature dependence of the Raman mode is shown in a magnified scale in Fig. 3(c). The Raman mode emerges around 300 K and grows in intensity as temperature is lowered. The originally infrared-active bending mode seems to be activated in the Raman spectra below 300 K. In a centrosymmetric crystal, in general, the infrared and Raman modes have, respectively, odd and even parities, and therefore the selection rule is orthogonal. The activation of the originally infrared modes in the Raman spectra implies the breaking of the space inversion symmetry below T_{CO2}. In fact, Tokunaga *et al.*[14] showed the electric polarization below T_{CO2} by measurement of the second-harmonic generation. Thus, the activation of the infrared mode in the Raman-scattering spectrum also confirms the COO-induced polar state in $Pr(Sr_{0.1}Ca_{0.9})_2Mn_2O_7$.

B. Charge-orbital order in $PrSr_2Mn_2O_7$ with the A-type magnetic ordering

In this section, we investigate the $d_{x^2-y^2}$ orbital ordered and A-type spin ordered state with a short-range vertical charge stripe order in $PrSr_2Mn_2O_7$ (Ref. 13) in terms of the optical conductivity spectra. Figure 5 shows optical conductivity spectra at various temperatures in $PrSr_2Mn_2O_7$. Spiky structures below 0.08 eV are due to optical-phonon modes. A gaplike structure as large as 0.15–0.25 eV is observed in a whole temperature region. A similar pseudogap formation was already reported for $La_{2-2x}Sr_{1+2x}Mn_2O_7$.[34] The magnitude of the charge gap is estimated by the extrapolation to the base line of $\sigma(\omega)=0$, as exemplified in the inset of Fig. 5; the value (2Δ) is plotted as a function of the temperature in Fig. 8(a). The gap magnitude is approximately constant $(2\Delta\simeq 0.25$ eV) above the antiferromagnetic transition temperature T_N, then gradually decreasing with decreasing temperature from T_N and saturated below 30 K. The decrease in the gap magnitude below T_N is caused by the xy plane electron delocalization in the A-type antiferromagnetic (i.e., in-plane ferromagnetic) state. Nevertheless, the complete clos-

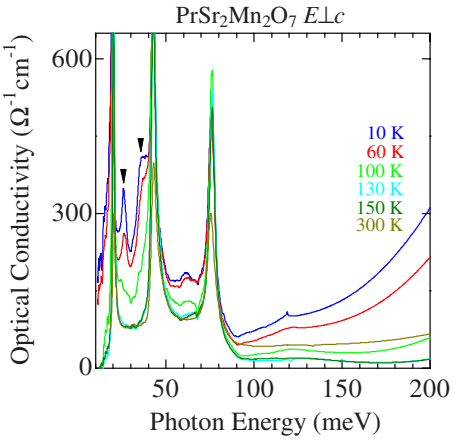

FIG. 6. (Color online) Optical conductivity spectra for $PrSr_2Mn_2O_7$ ($y=0$) at various temperatures. Closed triangles indicate the phonon modes activated by the formation of the vertical stripe ordering.

ing of the gap is not achieved even at the lowest temperature. In the related compound $La_{2-2x}Sr_{1+2x}Mn_2O_7$ ($x\sim0.5$),[34] the CE-COO and the A-type AF are reported to coexist. Therefore, there is some ambiguity regarding the origin of the observed gap (or pseudogap) structure. In the case of the present $Pr(Sr_{1-y}Ca_y)_2Mn_2O_7$ system, by contrast, these two charge-orbital ordering states are discriminated by the first-order phase transition line around $y=0.4$ as shown in Fig. 1(a). Therefore, the observed gap structure in $PrSr_2Mn_2O_7$ can be uniquely ascribed to the vertical stripe charge order. The vertical stripe charge order seems to suppress the coherent carrier motion and produce the gap structure. We show the optical conductivity spectra in Fig. 6 to scrutinize the low-energy region. The low-energy spectra in the high-temperature region above T_N are composed of three phonon modes, namely, stretching, bending, and external modes, and show little temperature variation. Below T_N, however, the continuum absorption evolves over the phonon energy region with decreasing temperature, indicating the delocalization of electrons by the in-plane ferromagnetic spin configuration. Simultaneously, two distinct phonon modes indicated by triangles increase their intensity with decreasing temperature.

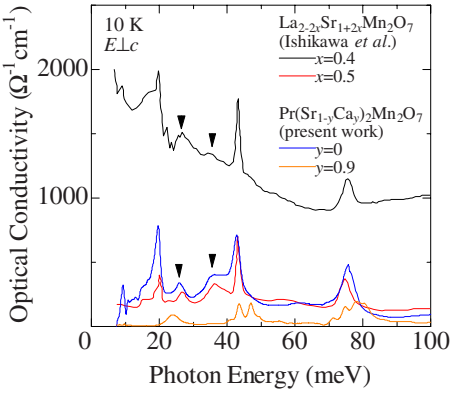

FIG. 7. (Color online) Comparison between optical conductivity spectra (Ref. 34) for $La_{2-2x}Sr_{1+2x}Mn_2O_7$ ($x=0.4,0.5$) reproduced from Ref. 34 and $Pr(Sr_{1-y}Ca_y)_2Mn_2O_7$ ($y=0,0.9$) at 10 K.

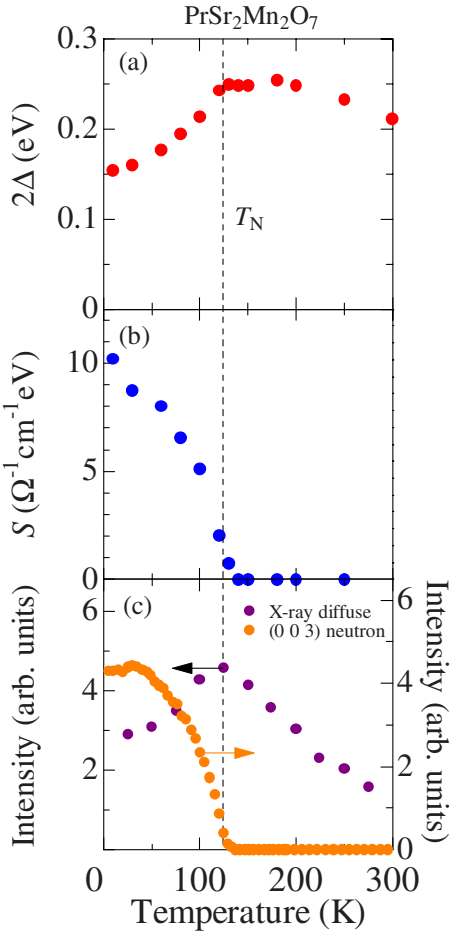

FIG. 8. (Color online) Temperature dependence of (a) the magnitude of the charge gap, (b) the oscillator strength of activated infrared phonon mode around 26 meV, and (c) the peak intensities of magnetic neutron Bragg (003) reflections for A-type spin order and the x-ray diffuse scattering peak intensities (Ref. 13) relevant to the vertical stripe-type charge ordering (reproduced from Ref. 13) for $PrSr_2Mn_2O_7$ ($y=0$).

This implies the lowering of lattice symmetry.

A gap or pseudogap structure as well as the activated far-infrared phonon modes were reported for $La_{2-2x}Sr_{1+2x}Mn_2O_7$ with $x=0.4$ and 0.5.[34] Figure 7 compares low-energy spectra of $PrSr_2Mn_2O_7$ with those of $La_{2-2x}Sr_{1+2x}Mn_2O_7$. The observed activated phonon modes are quite similar to those in $La_{2-2x}Sr_{1+2x}Mn_2O_7$, notably even in the metallic compound ($x=0.4$). The x-ray diffraction intensities of the vertical stripe charge order as well as the intensities of neutron magnetic Bragg spot due to the A-type AF for $PrSr_2Mn_2O_7$ are reproduced in Fig. 8(c).[13] The x-ray intensity can be observed even at room temperature and increases with decreasing temperature down to T_N but rather decreases toward lower temperature below T_N. Its temperature variant is similar to that of the gap magnitude shown in Fig. 8(a). Therefore, the origin of gap formation can be ascribed to the charge ordering or charge density wave in the present fully spin-polarized (in-plane ferromagnetic) and orbital-polarized (ferroic x^2-y^2) state. A most plausible origin of the activated phonon mode is the lattice distortion accompanied by the vertical charge stripe correlation. Nevertheless,

the temperature dependence of the activated phonon spectral intensity is quite different from that of the x-ray diffuse scattering; it is rather parallel with the evolution of the long-range magnetic order as represented by the (003) neutron diffraction [see Fig. 8(c)]. Perhaps, the lattice distortion caused by the vertical stripe charge order is too weak to be observed in the optical spectra above T_N. Below T_N, the phonon mode caused by the lattice distortion seems to gain the oscillator strength as a result of the Fano-type coupling with the underlying electronic continuum.

IV. CONCLUSION

We have investigated the optical spectra of the bilayered manganites $Pr(Sr_{0.1}Ca_{0.9})_2Mn_2O_7$ with the CE-COO and $PrSr_2Mn_2O_7$ with the A-type AF, uniform $d_{x^2-y^2}$ orbital, and vertical stripe charge order. In $Pr(Sr_{0.1}Ca_{0.9})_2Mn_2O_7$, we have observed an originally infrared-active optical-phonon mode in the Raman spectra below T_{CO2}. The appearance of the infrared modes in the Raman spectra indicates the breaking of the space inversion symmetry as a result of the ferroelectric state below T_{CO2}. A two-magnon band has also been discerned in the CE-type spin state. In $PrSr_2Mn_2O_7$, we have observed a charge gap structure as large as 150 meV in optical conductivity spectra. In the far-infrared region, two-phonon modes are activated below T_N. We have ascribed such a gap feature and activated phonon modes to the vertical charge stripe correlation that was verified by a former diffraction study.[13]

[1] Y. Tokura, Rep. Prog. Phys. **69**, 797 (2006).
[2] Y. Murakami, H. Kawada, H. Kawata, M. Tanaka, T. Arima, Y. Moritomo, and Y. Tokura, Phys. Rev. Lett. **80**, 1932 (1998).
[3] Z. Jirák, S. Krupička, Z. Šimša, M. Dlouhá, and S. Vratislav, J. Magn. Magn. Mater. **53**, 153 (1985).
[4] H. Kawano, R. Kajimoto, H. Yoshizawa, Y. Tomioka, H. Kuwahara, and Y. Tokura, Phys. Rev. Lett. **78**, 4253 (1997).
[5] R. Kajimoto, H. Yoshizawa, H. Kawano, H. Kuwahara, Y. Tokura, K. Ohoyama, and M. Ohashi, Phys. Rev. B **60**, 9506 (1999).
[6] T. Kimura, R. Kumai, Y. Tokura, J. Q. Li, and Y. Matsui, Phys. Rev. B **58**, 11081 (1998).
[7] K. Hirota, Y. Moritomo, H. Fujioka, M. Kubota, H. Yoshizawa, and Y. Endoh, J. Phys. Soc. Jpn. **67**, 3380 (1998).
[8] D. N. Argyriou, J. F. Mitchell, P. G. Radaelli, H. N. Bordallo, D. E. Cox, M. Medarde, and J. D. Jorgensen, Phys. Rev. B **59**, 8695 (1999).
[9] M. Kubota, H. Yoshizawa, Y. Moritomo, H. Fujioka, K. Hirota, and Y. Endoh, J. Phys. Soc. Jpn. **68**, 2202 (1999).
[10] C. D. Ling, J. E. Millburn, J. F. Mitchell, D. N. Argyriou, J. Linton, and H. N. Bordallo, Phys. Rev. B **62**, 15096 (2000).
[11] M. Kubota, H. Fujioka, K. Hirota, K. Ohoyama, Y. Moritomo, H. Yoshizawa, and Y. Endoh, J. Phys. Soc. Jpn. **69**, 1606 (2000).
[12] J. F. Mitchell, D. N. Argyriou, A. Berger, K. E. Gray, R. Osborn, and U. Welp, J. Phys. Chem. B **105**, 10731 (2001).
[13] Y. Tokunaga, T. J. Sato, M. Uchida, R. Kumai, Y. Matsui, T. Arima, and Y. Tokura, Phys. Rev. B **77**, 064428 (2008).
[14] Y. Tokunaga, T. Lottermoser, Y. S. Lee, R. Kumai, M. Uchida, T. Arima, and Y. Tokura, Nature Mater. **5**, 937 (2006).
[15] M. Kubota, Y. Oohara, H. Yoshizawa, H. Fujioka, K. Shimizu, K. Hirota, Y. Moritomo, and Y. Endoh, J. Phys. Soc. Jpn. **69**, 1986 (2000).
[16] L. Vasiliu-Doloc, S. Rosenkranz, R. Osborn, S. K. Sinha, J. W. Lynn, J. Mesot, O. H. Seeck, G. Preosti, A. J. Fedro, and J. F. Mitchell, Phys. Rev. Lett. **83**, 4393 (1999).
[17] Y.-D. Chuang, A. D. Gromko, D. S. Dessau, T. Kimura, and Y. Tokura, Science **292**, 1509 (2001).
[18] M. Imada, A. Fujimori, and Y. Tokura, Rev. Mod. Phys. **70**, 1039 (1998).
[19] K. Tobe, T. Kimura, and Y. Tokura, Phys. Rev. B **67**, 140402 (2003).
[20] K. Yamamoto, T. Kimura, T. Ishikawa, T. Katsufuji, and Y. Tokura, Phys. Rev. B **61**, 14706 (2000).
[21] E. Saitoh, Y. Tomioka, T. Kimura, and Y. Tokura, J. Phys. Soc. Jpn. **69**, 2403 (2000).
[22] K. Yamamoto, T. Kimura, T. Ishikawa, T. Katsufuji, and Y. Tokura, J. Phys. Soc. Jpn. **68**, 2538 (1999).
[23] Y. Tokunaga, R. Kumai, N. Takeshita, Y. Kaneko, J. P. He, T. Arima, and Y. Tokura, Phys. Rev. B **78**, 155105 (2008).
[24] E. Saitoh, S. Okamoto, K. T. Takahashi, K. Tobe, K. Yamamoto, T. Kimura, S. Ishihara, S. Maekawa, and Y. Tokura, Nature (London) **410**, 180 (2001).
[25] R. R. P. Singh, P. A. Fleury, K. B. Lyons, and P. E. Sulewski, Phys. Rev. Lett. **62**, 2736 (1989).
[26] K. Yamamoto, T. Katsufuji, T. Tanabe, and Y. Tokura, Phys. Rev. Lett. **80**, 1493 (1998).
[27] K. Yamamoto, K. Ishizaka, E. Saitoh, S. Shinomori, T. Tanabe, T. Katsufuji, and Y. Tokura, Phys. Rev. B **67**, 014414 (2003).
[28] H. L. Liu, S. Yoon, S. L. Cooper, G. Cao, and J. E. Crow, Phys. Rev. B **60**, R6980 (1999).
[29] D. Senff, F. Krüger, S. Scheidl, M. Benomar, Y. Sidis, F. Demmel, and M. Braden, Phys. Rev. Lett. **96**, 257201 (2006).
[30] Y. Okimoto, T. Katsufuji, T. Ishikawa, T. Arima, and Y. Tokura, Phys. Rev. B **55**, 4206 (1997).
[31] S. K. Park, T. Ishikawa, Y. Tokura, J. Q. Li, and Y. Matsui, Phys. Rev. B **60**, 10788 (1999).
[32] T. Katsufuji, T. Tanabe, T. Ishikawa, Y. Fukuda, T. Arima, and Y. Tokura, Phys. Rev. B **54**, R14230 (1996).
[33] T. Ishikawa, S. K. Park, T. Katsufuji, T. Arima, and Y. Tokura, Phys. Rev. B **58**, R13326 (1998).
[34] T. Ishikawa, K. Tobe, T. Kimura, T. Katsufuji, and Y. Tokura, Phys. Rev. B **62**, 12354 (2000).